NANO LETTERS

pubs.acs.org/NanoLett Letter

Customizing Radiative Decay Dynamics of Two-Dimensional Excitons via Position- and Polarization-Dependent Vacuum-Field Interference

Sanghyeok Park,◆ Dongha Kim,◆ Yun-Seok Choi, Arthur Baucour, Donghyeong Kim, Sangho Yoon, Kenji Watanabe, Takashi Taniguchi, Jonghwa Shin, Jonghwan Kim, and Min-Kyo Seo*

Cite This: https://doi.org/10.1021/acs.nanolett.2c04604 Read Online

ACCESS | Metrics & More | Article Recommendations | Supporting Information

ABSTRACT: Embodying bosonic and interactive characteristics in two-dimensional space, excitons in transition metal dichalcogenides (TMDCs) have garnered considerable attention. The utilization of the strong-correlation effects, long-range transport, and valley-dependent properties requires customizing exciton decay dynamics. Vacuum-field manipulation allows radiative decay engineering without disturbing intrinsic material properties. However, conventional flat mirrors cannot customize the radiative decay landscape in TMDC's plane or support vacuum-field interference with desired spectrum and polarization properties. Here, we present a meta-mirror platform resolving the issues with more optical degrees of freedom. For neutral excitons of the monolayer $MoSe_2$, the optical layout formed by meta-mirrors manipulated the radiative decay rate in space by 2 orders of magnitude and revealed the statistical correlation between emission intensity and spectral line width. Moreover, the anisotropic meta-mirror demonstrated polarization-dependent radiative decay control. Our platform would be promising to tailor two-dimensional distributions of lifetime, density, diffusion, and polarization of TMDC excitons in advanced opto-excitonic applications.

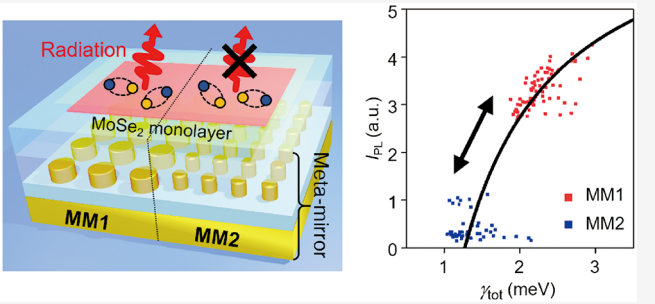

KEYWORDS: *excitons, transition metal dichalcogenide, radiative decay dynamics, meta-mirror, vacuum-field interference*

Excitons, quasi-particles of bounded electron−hole pairs, have appealed as a fascinating platform for quantum many-body phenomena and optoelectronic devices with their bosonic and interactive characteristics.[1] In monolayer transition metal dichalcogenides (TMDCs), inversion/time-reversal symmetry breaking and reduced dielectric screening provide outstanding features for excitons, such as massive binding energy, high quantum efficiency, and valley properties, which opened a new era in fundamental studies and applications of excitons.[2] One significant breakthrough is the realization of exotic strongly correlated phenomena, including Bose−Einstein condensation,[3] superfluidity,[4,5] Wigner crystals,[6−9] and excitonic insulators.[10] Outstanding excitonic/optoelectronic applications, such as long-range exciton transport devices,[11−14] room-temperature excitonic transistors,[15] valleytronic devices,[16−18] bright single-photon sources,[19,20] and excitonic lasers,[21,22] have also been demonstrated. The key to their success lies in the lifetime engineering of two-dimensional excitons, which should be tuned from picosecond[20,23] (for conventional optoelectronics) to sub-microsecond[13,24] (for strongly correlated systems and advanced excitonics) time scales.

Lifetime engineering of two-dimensional excitons has been intensively investigated using various approaches. In terms of materials, the engineering of exciton decay dynamics by an order of magnitude has typically been realized by strain,[25,26] defect implantation,[27] and electrostatic biasing.[24,28,29] However, these methods are accompanied by undesired outcomes, such as changes in the exciton binding energy and electronic band gap, formation of exciton complexes, and stimulation of nonradiative decay channels. Meanwhile, optical methods engineering the vacuum field by the Purcell effects have been recently proposed to manipulate the radiative decay dynamics of excitons in a purely environmental manner without affecting their inherent properties. Planar metallic mirrors and dielectric distributed Bragg reflectors (DBRs) have attracted much attention in boosting and controlling light−matter interactions at the weak-[30−33] and strong-coupling regimes[34−36] while maintaining the two-dimensional characteristics and degrees of freedom of TMDC excitons. However, the conventional planar

Received: November 22, 2022
Revised: February 20, 2023

https://doi.org/10.1021/acs.nanolett.2c04604
Nano Lett. XXXX, XXX, XXX−XXX

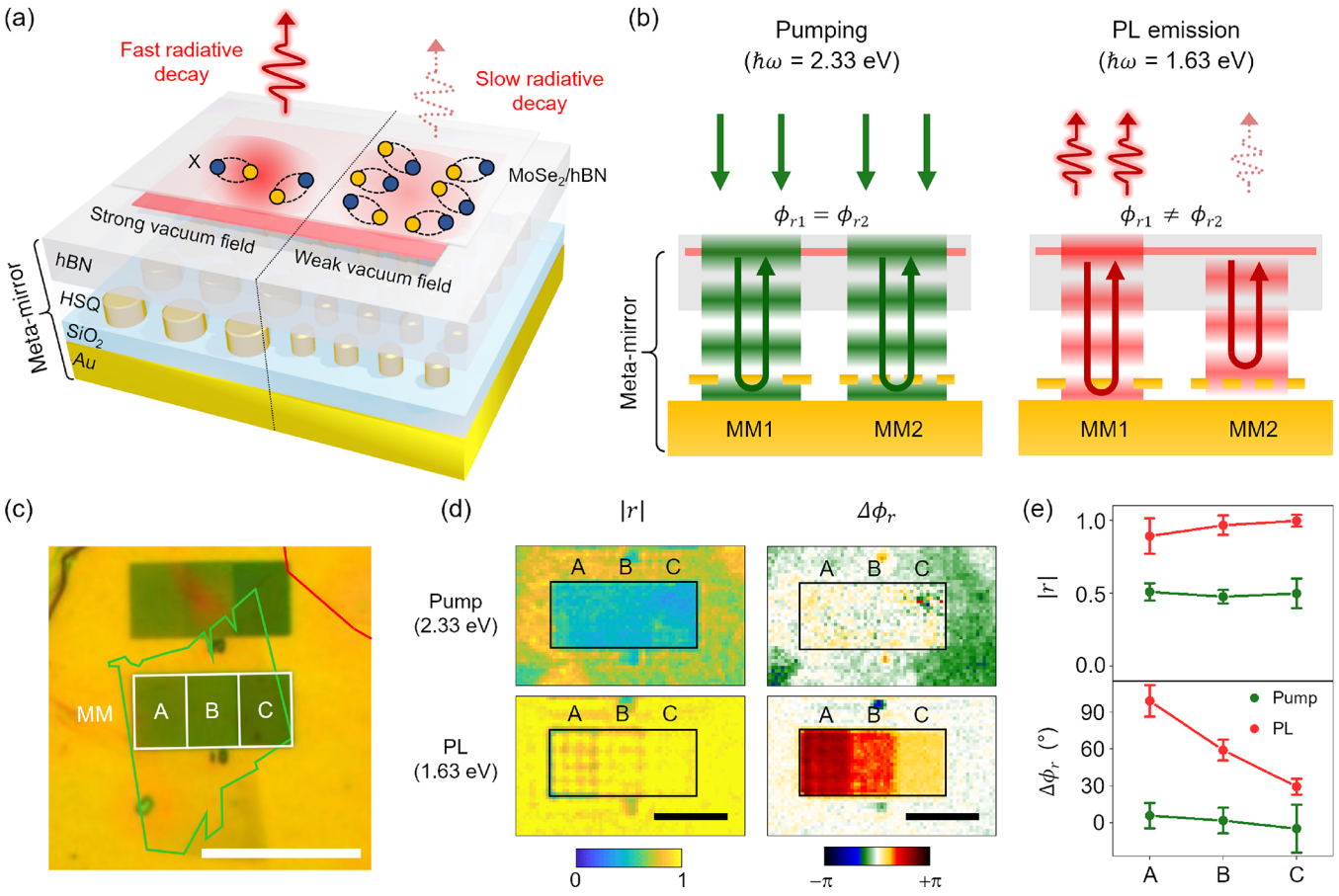

Figure 1. Engineering the vacuum-field interference and exciton decay dynamics by the meta-mirror platform. (a, b) Schematic illustration and mechanism of the radiative decay control of excitons in the meta-mirror platform. By controlling the vacuum field in the plane of the TMDC layer, the meta-mirror customizes the two-dimensional landscape of the radiative decay and density of excitons. We present two representative meta-mirrors, MM1 and MM2, that support the same reflection phases ($\phi_{r1} = \phi_{r2}$) at the pumping frequency but different reflection phases ($\phi_{r1} \neq \phi_{r2}$) at the PL emission frequency. When the reflection amplitude is the same, the pumping condition is identical, but the Purcell effect on the radiative decay of PL emission is considerably different. (c) Optical microscope image of the $MoSe_2$ monolayer (green solid polygon) on the meta-mirrors (white rectangles). The red solid line is a part of the boundary of the encapsulating hBN flake. Scale bar: 20 μm. (d) Measured distribution of the reflection amplitude $|r|$ and the relative reflection phase $\Delta\phi_r$ of the meta-mirrors at the pumping ($\hbar\omega$ = 2.33 eV) and emission (1.63 eV) frequency. Scale bar: 10 μm. (e) Reflection amplitude and relative reflection phase averaged over the area of each meta-mirror A, B, and C for the pumping and PL emission frequencies. The error bars indicate the standard deviations of the reflection amplitude and relative phase measured over each meta-mirror area.

mirrors cannot provide the necessary functionalities in excitonic devices, such as spatial customization of the decay dynamics over the horizontal TMDC plane and independent control of the optical excitation and radiative decay of excitons. Such planar mirrors, which work depending on their distances from target emitters, cannot produce an inhomogeneous distribution of suppressed or enhanced vacuum fields within a single two-dimensional plane. Meanwhile, plasmonic nanostructures and metasurfaces have also been utilized for engineering the radiative decay dynamics of TMDC excitons but primarily focused on giant Purcell enhancement through strong field confinement[37,38] and featuring optical properties such as polarization, chirality, and orbital angular momentum.[39−42] However, unlike optoelectronic applications, the demonstration of quantum many-body phenomena and exciton diffusion/transport devices rather requires suppression of the radiative decay rate for long-lived excitons.[3−15]

Here we present optical customization of decay dynamics of two-dimensional excitons by assemblable, versatile plasmonic meta-mirrors. The meta-mirrors tailor the local distribution and spectral/polarization properties of the optical vacuum field in the plane of the employed TMDC material, depending on their geometry and arrangement.[43] Owing to the sub-wavelength-scale size and periodicity of its meta-atoms, the meta-mirror enables us to precisely shape the two-dimensional landscape of the decay rate and density of the TMDC excitons with respect to their micrometer-scale diffusion length. In the experiments, our meta-mirror platform was seamlessly integrated with the $MoSe_2$ monolayer without affecting the intrinsic properties of the excitons and manipulated the radiative decay rate of the neutral excitons spatially by 2 orders of magnitude. We were thus able to systematically identify the correlation between the photoluminescence (PL) intensity and spectral line width of the $MoSe_2$ monolayer's neutral excitons. Accordingly, we observed the Lamb shift in cooperation with the optical vacuum field. In addition, we demonstrated the polarization-dependent customization of the radiative decay dynamics of excitons using the anisotropic meta-mirror, which is a representative example of the abilities

https://doi.org/10.1021/acs.nanolett.2c04604
Nano Lett. XXXX, XXX, XXX−XXX

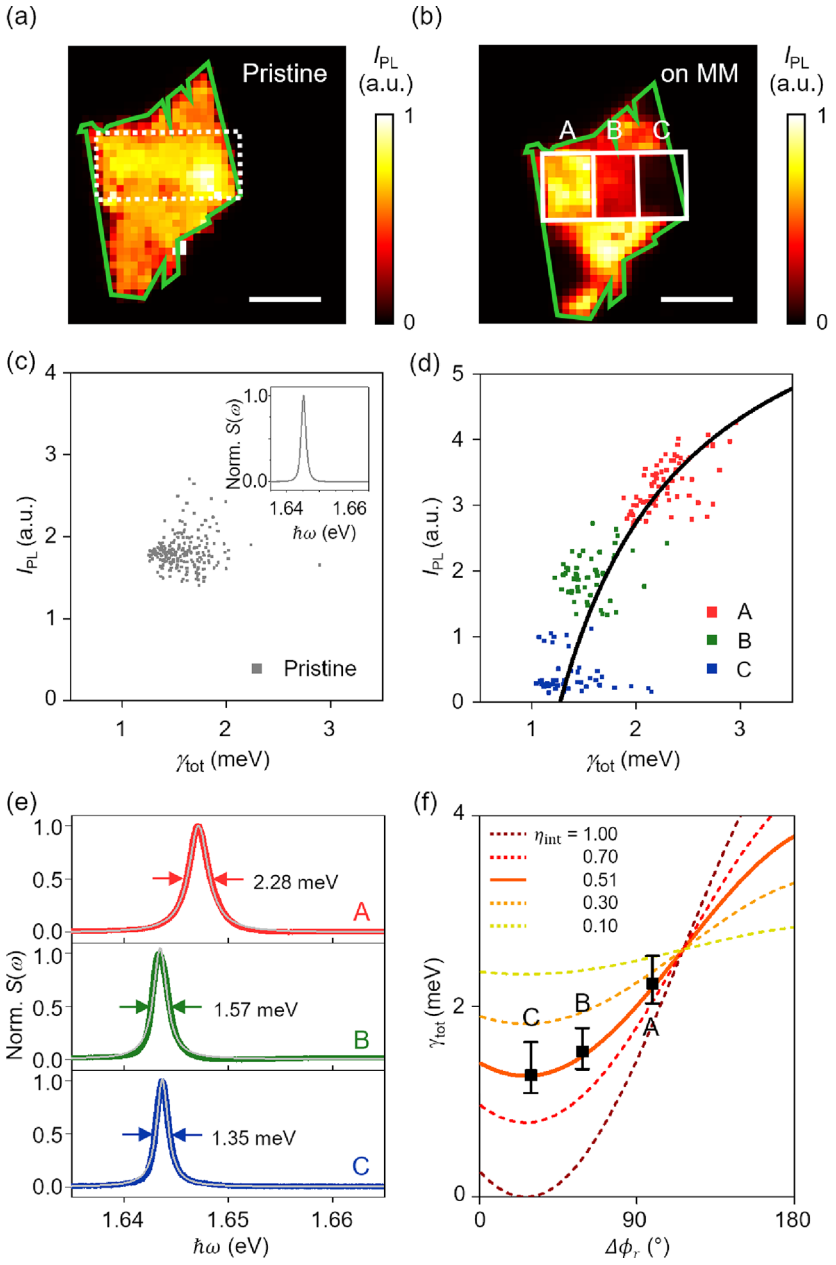

Figure 2. Manipulation of radiative decay dynamics of neutral excitons. (a, b) PL intensity distribution of neutral excitons of the hBN-encapsulated $MoSe_2$ monolayer on the Si/SiO_2 substrate (pristine) and the meta-mirrors. The green and white outlines indicate the region of the $MoSe_2$ monolayer and the meta-mirrors, respectively. Scale bar: 10 μm. (c, d) Scatter plots of the intensity (I_{PL}) and line width (γ_{tot}) of the neutral exciton PL spectrum on (c) the Si/SiO_2 substrate and (d) meta-mirrors A, B, and C. The representative neutral exciton PL spectrum of the pristine $MoSe_2$ monolayer is shown in the inset of (c). $S(\omega)$ represents the normalized spectral density. (e) Representative PL emission spectra of the neutral exciton engineered by the meta-mirror A, B, and C (the red, green, and blue solid lines, respectively). The fitted Lorentzian curves are depicted with the solid gray lines. (f) Results of the model analysis on the total decay rate (γ_{tot}) depending on the relative reflection phase shift ($\Delta\phi_r$). By employing the coherent optical feedback model, we calculated γ_{tot} for different internal quantum efficiencies (η_{int}). The model with η_{int} = 0.51 yields the best fit (the solid orange line) to the experimental measurements (the black squares and error bars).

of meta-surfaces and meta-materials to dress TMDC excitonic devices with sophisticated optical functionalities.[39−45]

The meta-mirror consists of a Au bottom mirror, an SiO_2 spacer, a Au nanodisk array, a spin-coated hydrogen silsesquioxane (HSQ) superstrate, and a hexagonal boron nitride (hBN) layer (Figure 1a). TMDC materials are located on top of the hBN layer of the meta-mirror and might be covered by another thin hBN layer (Supporting Information Section S1). Depending on the radius and period of the Au nanodisks, the plasmonic meta-mirror reflects the incident light with different phases at the pumping and exciton emission frequencies (Supporting Information Section S2). We designed the meta-mirrors to engineer the Purcell effects on the plane of the $MoSe_2$ monolayer based on the coherent optical feedback model.[30−33] We optimized the thickness of the SiO_2 spacer to determine the combination of the radius and period of the Au nanodisks, which supports an identical reflection amplitude at a given frequency of light. The reflection phase (ϕ_r) and amplitude ($|r|$) of the light determine the vacuum-field interference in the plane of interest along the vertical direction,

https://doi.org/10.1021/acs.nanolett.2c04604
Nano Lett. XXXX, XXX, XXX−XXX

including the top surface of the meta-mirror. The stronger the vacuum field, the faster will be the radiative decay, and the lower will be the density of excitons. By arranging different meta-mirrors, we can yield two-dimensional lithography of the exciton density. A schematic illustration of two representative meta-mirrors (MM1 and MM2) that operate identically for pumping but distinctly for emission is depicted in Figure 1b. At the pumping frequency, MM1 and MM2 possess the same reflection amplitude and phase ($\phi_{r1} = \phi_{r2}$) and support identical interference between the incident and reflected light. At the emission frequency, MM1 and MM2 reflect the incident light with the same amplitude but different phases ($\phi_{r1} \neq \phi_{r2}$). Depending on the reflection phase, the vacuum-field interference at the PL emission frequency can be controlled between constructive and destructive conditions.

For the experiment, we prepared three different plasmonic meta-mirrors (A, B, and C) to demonstrate optical customization of the radiative decay dynamics of excitons (Figure 1c and Supporting Information Section S3). The spin-coated HSQ superstrate gets rid of the surface fluctuation from the Au nanodisk array and minimized the local strain effects on the employed two-dimensional material (Supporting Information Section S4). We targeted the neutral excitons of the monolayer $MoSe_2$, of which the photoluminescence (PL) emission frequency was 1.63 eV, and the pumping frequency was 2.33 eV. The reflection amplitude and phase of the meta-mirrors were examined by off-axis holography (Figure 1d and Supporting Information Section S1). Here, we measured the reflection phase shift ($\Delta\phi_r$) of the meta-mirror relative to that of the region without Au nanodisks. At the pumping frequency, the three meta-mirrors demonstrated approximately the same reflection amplitude and reflection phase, ensuring identical exciton excitations. However, at the PL emission frequency, the reflection phase exhibits a stepwise change among the different meta-mirrors while maintaining the reflection amplitude proximate to unity. Notably, the higher the reflection amplitude, the higher will be the visibility of the vacuum-field interference, and the higher will be the dynamic range in the radiative decay engineering (Supporting Information Section S5). The reflection amplitude and relative phase averaged over the area of each meta-mirror are plotted in Figure 1e. The reflection amplitudes of the meta-mirrors A, B, and C at the PL emission frequency were measured to be 0.89, 0.96, and 0.99, respectively. The relative reflection phase at the PL emission frequency changes by 69.47°, from 29.49° to 98.96°. The standard deviation of the measured reflection amplitude and relative phase serves as an indicator of the spatial uniformity of the meta-mirror's performance. A phase change of π is required for covering all ranges between the constructive and destructive interference of the vacuum field. The numerical calculations of the meta-mirror indicate that a maximum relative phase change of 269.59° can be achieved, depending on the radius and period of the Au nanodisks (Supporting Information Section S2). We also examined the performance of the finite-sized meta-mirror depending on its size and found that finite-sized meta-mirrors with a side length of ~2 μm exhibit similarity in performance to the infinite meta-mirrors (Supporting Information Section S6).

The meta-mirror enables robust control of the radiative recombination of excitons and the two-dimensional arrangement of areas featuring different properties of radiative decay. By employing a confocal microscopy setup (Supporting Information Section S1), we initially measured the PL intensity (I_{PL}) distribution of the $MoSe_2$ monolayer's neutral excitons on the Si/SiO_2 substrate and the three neighboring meta-mirrors presented in Figure 1c–e. We prepared the $MoSe_2$ monolayer flake encapsulated by the hBN layers with thicknesses of 6 and 174 nm, of which the thicker layer is the top layer of the meta-mirror platform. The $MoSe_2$ monolayer, placed on an Si/SiO_2 substrate, exhibits uniform PL over its entire area (Figure 2a). However, after transfer onto the meta-mirrors, the PL intensity varies significantly and sharply for each meta-mirror (Figure 2b). The ratio of the averaged PL intensities on the three different meta-mirrors (A, B, and C) is 9.78:4.70:1.00. Considering that the employed meta-mirrors support pumping conditions that are approximately identical (Figure 1d,e), the manipulation of the vacuum-field interference at the emission frequency dominates the difference in the PL intensity. The three meta-mirrors enabled the control of the vacuum field and exciton PL emission intensity by 1 order of magnitude. In addition, the arrangement of different meta-mirrors provides a platform to spatially engineer light-matter interaction properties in two dimensions as desired, beyond the limits of typical planar mirrors.

To further reveal changes in the radiative decay dynamics of neutral excitons via vacuum-field interference manipulation, we statistically analyzed the intensity and line width of the PL spectrum of the $MoSe_2$ monolayer on the SiO_2/Si substrate (white dashed rectangle in Figure 2a) and the meta-mirrors (white solid rectangles in Figure 2b). By fitting the measured PL spectrum with the Lorentzian function, we have precisely determined the spectral line width, which corresponds to the total decay rate (γ_{tot}) of excitons. As plotted in Figure 2c, the pristine $MoSe_2$ monolayer on the SiO_2/Si substrate exhibits an ordinary statistical distribution in which the line width is 1.58 ± 0.21 meV. The center frequency of the neutral exciton emission of the pristine $MoSe_2$ monolayer is 1.645 eV (the inset of Figure 2c). However, the statistics of the PL spectra on the meta-mirrors indicate a high correlation between the PL intensity and line width, as demonstrated in Figure 2d. The meta-mirrors A, B, and C result in distinct line widths of 2.24, 1.53, and 1.28 meV in median, respectively, which reflect the change in the exciton lifetime owing to the manipulation of the vacuum-field interference. We expect that our meta-mirrors can cater to different needs, depending on the research purpose; for example, optical exciton reading/writing with meta-mirror A, long-range exciton transport with meta-mirror C, or even a lateral combination of both in a two-dimensional space. Moreover, the standard deviations of the PL line widths measured on the meta-mirror A, B, and C are 0.25, 0.22, and 0.27 meV, respectively, and their values normalized to the averaged line widths are 10.88%, 13.82%, and 19.61%. Considering that the normalized standard deviation of the PL line width of the pristine $MoSe_2$ monolayer on the SiO_2/Si substrate was 13.15%, the meta-mirrors seamlessly preserved the inherent properties of the two-dimensional material. It has been known that undesired creations of material factors such as detects, strain, deformations, and electrostatic doping can affect the decay channels of excitons locally and increase spatial inhomogeneity in the PL intensity and line shape.[25,29,46] Figure 2e shows the representative PL spectra of neutral excitons engineered by the meta-mirrors A, B, and C. We expect that the slight emission frequency change of ~3.7 meV originated from the cooperative Lamb shift[31] owing to the coherent

https://doi.org/10.1021/acs.nanolett.2c04604
Nano Lett. XXXX, XXX, XXX−XXX

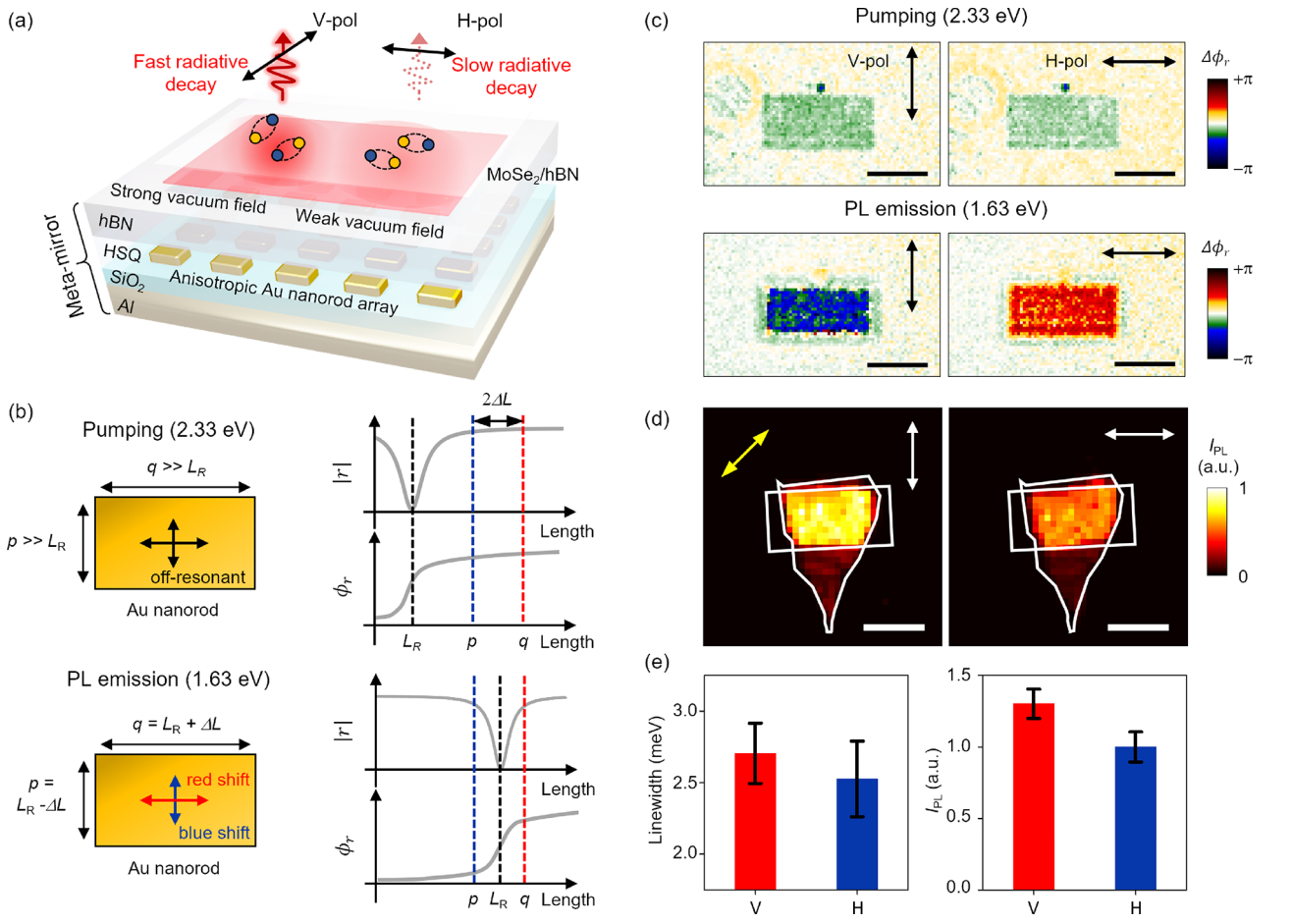

Figure 3. Polarization-dependent control of exciton radiative decay dynamics. (a) Schematic illustration of the anisotropic meta-mirror for assigning the linear-polarization dependency to the radiative decay dynamics of the TMDC excitons. (b) Plasmonic response of the Au nanorod of the anisotropic meta-mirror. L_R symbolizes the length required for the Au nanorod to support the localized plasmon resonance. Depending on the choice of the length (q) and width (p) of the Au nanorod with respect to L_R, we can independently engineer the reflection phases for the H- and V-polarization states. ΔL represents half of the difference between p and q. (c) Distribution of the relative reflection phase of the anisotropic meta-mirror at the pumping and emission frequency for the H- and V-polarization. Scale bar: 10 μm. (d) Measured PL emission intensity distribution of neutral excitons on the anisotropic meta-mirror for the V- (left panel) and H- (right panel) polarization state. The yellow arrow indicates the polarization of the pumping light. Scale bar: 10 μm. (e) Measured PL spectrum line width (left panel) and intensity (right panel) of the neutral exciton emission depending on the polarization state.

interaction between the vacuum-field fluctuations and excitons (Supporting Information Section S7).

The measured PL statistics can be theoretically modeled by considering coherent optical feedback.[30−33] The reflection amplitude and phase pickup by the meta-mirror control the local density of optical states and the Purcell factor (F_P) at the $MoSe_2$ monolayer, leading to the total decay rate of excitons being expressed as $\gamma_{tot} = \gamma_{nrad} + F_P\gamma_{rad,0} = \gamma_{tot,0}[1 + \eta_{int}|r|\cos(\phi_r)]$, where η_{int} represent the internal quantum efficiency of radiative recombination (Supporting Information Section S5). The internal quantum efficiency relates the intrinsic total and radiative decay rates, $\gamma_{tot,0}$ and $\gamma_{rad,0}$, respectively, of the monolayer $MoSe_2$ as $\gamma_{rad,0} = \eta_{int}\gamma_{tot,0}$. Figure 2f depicts the theoretical and experimental results for the total decay rate as a function of the measured relative reflection phase. The model analysis of the measured total decay rates extracted the internal quantum efficiency and nonradiative decay rate (γ_{nrad}) of $MoSe_2$ monolayer's excitons to be 0.51 and 1.27 meV in median, respectively. The extracted nonradiative decay rate explains the correlation between the PL intensity and line width following $I_{PL} \propto \gamma_{rad}/\gamma_{tot} = (\gamma_{tot} - \gamma_{nrad})/\gamma_{tot}$ (the black solid curve in Figure 2d). Considering the extracted nonradiative decay rate, meta-mirrors A, B, and C modify the radiative decay rate, $\gamma_{rad} = F_P\gamma_{rad,0}$, from 0.97, 0.26, and 0.01 meV. Moreover, as demonstrated by its radiative and total decay rates, meta-mirror C suppresses the vacuum field to a near-zero value and causes the exciton lifetime to approach the nonradiative decay limit. The coherent feedback model also effectively predicts the changes in the PL intensity engineered by the meta-mirrors (Supporting Information Section S5). We expect that the meta-mirror platform combined with high-quality TMDC can support long-lived intralayer excitons for long-range interactions[3−9] and transport[11−15] with high-quality TMDCs.

The meta-mirror brings its polarization-dependent features to the radiative decay dynamics of excitons in the $MoSe_2$ monolayer. A meta-mirror consisting of anisotropic meta-atoms manipulates the vacuum-field interference depending on the polarization state (Figure 3a). Upon employing the Au nanorods as meta-atoms, the exciton PL emission exhibits different radiative decay rates for the horizontal (H) and vertical (V) polarization states. Figure 3b shows the

https://doi.org/10.1021/acs.nanolett.2c04604
Nano Lett. XXXX, XXX, XXX−XXX

mechanism of polarization-dependent vacuum-field manipulation using the anisotropic meta-mirror. Depending on its length (q) and width (p), the anisotropic Au nanorod supports localized surface plasmon resonance (LSPR) at different frequencies for the H- and V-polarization states. The higher the frequency of light, the longer will be the length/width for LSPR (L_R): L_R of ∼20 and ∼100 nm for the pumping and PL emission frequencies (Supporting Information Section S8). For the pumping frequency, both p and q are sufficiently larger than L_R, and the off-resonance behavior causes a similar reflection amplitude and phase for the H- and V-polarized states. In contrast, for the emission frequency, the length (width) of the Au nanorod becomes larger (shorter) than L_R by an amount ΔL: $q = L_R + \Delta L$ and $p = L_R - \Delta L$. In this configuration, the Au nanorod reflects H- and V-polarized light with an equivalent reflectance but causes a significant difference in their reflection phases. Moreover, the relative phase difference can be easily tuned from the in-phase to out-of-phase conditions by changing the width and length. The high reflectance of the off-resonance state increases the visibility of the vacuum-field interference. We note that the meta-mirrors with the Al bottom mirror show a relatively high reflection amplitude at both pumping and emission wavelengths, while those with the Au bottom mirror are further optimized in the near-infrared range including the emission wavelength (Figure S13).

We measured the birefringent reflectance of the fabricated anisotropic meta-mirror using polarization-resolved off-axis holography (Figure 3c). The meta-mirror consists of 71 × 35 Au nanorods with a period of 280 nm (See Supporting Information Section S1). The length, width, and thickness of the Au nanorods are 110, 90, and 40 nm, respectively. At the pumping frequency, the reflection amplitude averaged over the meta-mirror was 0.82 ± 0.051 and 0.79 ± 0.050 for the H- and V-polarized states, respectively (Supporting Information Section S10), and the reflection phase difference is only ∼4.09°. The measured reflection amplitude and phase difference enable an approximately equivalent pumping condition independent of the polarization state. At the emission frequency, the reflection phase difference between the H- and V-polarized states is ∼128.06°, which shows nice consistency with the numerical calculation (Supporting Information Section S8). The relative phase difference between the V- and H-polarized states can be further increased up to ∼177.24° by precise optimization of the length and width of the anisotropic Au nanorod (Figure S12).

Subsequently, using the anisotropic meta-mirror, we demonstrated the polarization-dependent customization of the radiative decay of the neutral exciton in the $MoSe_2$ monolayer (Figure 3d). The polarization angle of the pumping light is 45°. The PL intensity of the V-polarized state is brighter than that of the H-polarized state inside the area of the meta-mirror. However, the PL intensity does not exhibit a notable difference outside the meta-mirror. We conducted a statistical analysis of the line width and intensity of the measured PL spectra depending on the polarization state, and the results are illustrated in Figure 3e. The measured line width is 2.70 ± 0.21 and 2.53 ± 0.26 meV for the V- and H-polarization states, respectively. The ratio of the PL emission intensity of the V- to H-polarization is ∼1.30. Based on the relation between the PL intensity and exciton decay rate, we revealed that the radiative decay rate for the H- and V-polarization states are 0.43 and 0.60 meV, respectively (Supporting Information Section S11). We further experimentally confirmed that the same polarization-dependent behavior of the line width/decay rate appears when the polarization of the pump light is set to be parallel to that of the emission light (Supporting Information Section S12).

In this study, we demonstrated a meta-mirror platform to customize the radiative decay rate of TMDC excitons and its two-dimensional distribution by manipulating the reflection phase and amplitude of the vacuum field as desired. In a purely optical manner, we controlled the radiative decay rate of the neutral excitons of the monolayer $MoSe_2$ by 2 orders of magnitude, which resulted in a significant variation of the spectral line width from 1.28 to 2.24 meV. The seamless integration of the meta-mirror platform and TMDC material without affecting the intrinsic properties of the excitons enabled the experimental identification of the correlation between the emission intensity and spectral line width and the observation of the Lamb shift. We expect that the application of the meta-mirror platform to time-resolved measurements[30,47] will further clarify the observed correlation between the PL intensity and line width. The anisotropic meta-mirror assigned polarization dependency to the radiative decay dynamics of the TMDC excitons. We expect that the position- and polarization-dependent customization of the radiative decay dynamics of excitons in two-dimensional space will be a promising approach for yielding exciton transport[11−15,48] and strong-correlation effects[3−9] with more optical degrees of freedom and demonstrate advanced photon−exciton transducers.[49,50]

■ ASSOCIATED CONTENT

Supporting Information

The Supporting Information is available free of charge at https://pubs.acs.org/doi/10.1021/acs.nanolett.2c04604.

Methods; numerical simulation of the reflection amplitude and phase of the meta-mirror; scanning electron microscope image of the meta-mirror; surface roughness of the spin-coated HSQ superstrate; analysis of radiative decay engineering using coherent optical feedback model; performance of finite-sized meta-mirror; statistics of the line width and center frequency of the neutral exciton PL spectrum; design of the anisotropic meta-mirror; adjusting performance of anisotropic meta-mirror depending on the material of bottom mirror; reflection amplitude and phase of the anisotropic meta-mirror; analysis of polarization-dependent radiative decay engineering via anisotropic meta-mirror; radiative decay dynamics depending on the polarization state of the pumping light; pumping power dependence of the neutral exciton PL line width (PDF)

■ AUTHOR INFORMATION

Corresponding Author

Min-Kyo Seo − *Department of Physics, Korea Advanced Institute of Science and Technology, Daejeon 34141, Republic of Korea;* orcid.org/0000-0003-0618-3955; Email: minkyo_seo@kaist.ac.kr

Authors

Sanghyeok Park − *Department of Physics, Korea Advanced Institute of Science and Technology, Daejeon 34141, Republic of Korea*

https://doi.org/10.1021/acs.nanolett.2c04604
Nano Lett. XXXX, XXX, XXX−XXX

Dongha Kim − *Department of Physics, Korea Advanced Institute of Science and Technology, Daejeon 34141, Republic of Korea*

Yun-Seok Choi − *Department of Chemistry, Korea Advanced Institute of Science and Technology, Daejeon 34141, Republic of Korea;* orcid.org/0000-0002-8583-0585

Arthur Baucour − *Department of Materials Science and Engineering, Korea Advanced Institute of Science and Technology, Daejeon 34141, Republic of Korea;* orcid.org/0000-0002-8251-5504

Donghyeong Kim − *Department of Physics, Korea Advanced Institute of Science and Technology, Daejeon 34141, Republic of Korea*

Sangho Yoon − *Department of Materials Science and Engineering, Pohang University of Science and Technology, Pohang 37673, Republic of Korea; Center for van der Waals Quantum Solids, Institute for Basic Science (IBS), Pohang 37673, Republic of Korea*

Kenji Watanabe − *Research Center for Functional Materials, National Institute for Materials Science, Tsukuba 305-0044, Japan;* orcid.org/0000-0003-3701-8119

Takashi Taniguchi − *International Center for Materials Nanoarchitectonics, National Institute for Materials Science, Tsukuba 305-0044, Japan;* orcid.org/0000-0002-1467-3105

Jonghwa Shin − *Department of Materials Science and Engineering, Korea Advanced Institute of Science and Technology, Daejeon 34141, Republic of Korea;* orcid.org/0000-0003-0712-464X

Jonghwan Kim − *Department of Materials Science and Engineering, Pohang University of Science and Technology, Pohang 37673, Republic of Korea; Center for van der Waals Quantum Solids, Institute for Basic Science (IBS), Pohang 37673, Republic of Korea*

Complete contact information is available at: https://pubs.acs.org/10.1021/acs.nanolett.2c04604

Author Contributions

◆S.P. and D.K. contributed equally to this paper. S.P., D.K., and M.-K.S. conceived the project. S.P., D.K., and A.B. fabricated the meta-mirrors. S.P., D.K., D.K., and S.Y. fabricated the two-dimensional heterostructures. S.P. and Y.-S.C. performed the optical phase measurements. S.P. performed the confocal PL measurements. S.P. and D.K. performed the theoretical calculations. K.W. and T.T. provided the boron nitride crystals. S.P., D.K., and M.-K.S. analyzed the data and wrote the manuscript with the assistance of all other authors.

Funding

M.-K.S. acknowledges support from the KAIST Cross-Generation Collaborative Lab project and the National Research Foundation of Korea (NRF) (2020R1A2C2014685 and 2020R1A4A2002828). J.K. acknowledges the support of the NRF (2020R1A2C2103166). J.S. acknowledges the support of the NRF (2021R1A2C2008687). D.K. acknowledges support from the NRF (2015H1A2A1033753). Y.-S.C. acknowledges support from the NRF (2020R1I1A1A01069219). K.W. and T.T. acknowledge support from JSPS KAKENHI (Grant Numbers 19H05790, 20H00354, and 21H05233) and A3 Foresight by JSPS.

Notes

The authors declare no competing financial interest.

REFERENCES

(1) Butov, L. V. Excitonic devices. *Superlattices Microstruct.* **2017**, *108*, 2−26.

(2) Mak, K. F.; Xiao, D.; Shan, J. Light−valley interactions in 2D semiconductors. *Nat. Photon* **2018**, *12*, 451−460.

(3) Wang, Z.; Rhodes, D. A.; Watanabe, K.; Taniguchi, T.; Hone, J. C.; Shan, J.; Mak, K. F. Evidence of high-temperature exciton condensation in two-dimensional atomic double layers. *Nature* **2019**, *574*, 76−80.

(4) Liu, X.; Li, J. I. A.; Watanabe, K.; Taniguchi, T.; Hone, J.; Halperin, B. I.; Kim, P.; Dean, C. R. Crossover between strongly coupled and weakly coupled exciton superfluids. *Science.* **2022**, *375*, 205−209.

(5) Arp, T. B.; Pleskot, D.; Aji, V.; Gabor, N. M. Electron−hole liquid in a van der Waals heterostructure photocell at room temperature. *Nat. Photonics* **2019**, *13*, 245−250.

(6) Smoleński, T.; Dolgirev, P. E.; Kuhlenkamp, C.; Popert, A.; Shimazaki, Y.; Back, P.; Lu, X.; Kroner, M.; Watanabe, K.; Taniguchi, T.; Esterlis, I.; Demler, E.; Imamoğlu, A. Signatures of Wigner crystal of electrons in a monolayer semiconductor. *Nature* **2021**, *595*, 53−57.

(7) Regan, E. C.; Wang, D.; Jin, C.; Bakti Utama, M. I.; Gao, B.; Wei, X.; Zhao, S.; Zhao, W.; Zhang, Z.; Yumigeta, K.; Blei, M.; Carlström, J. D.; Watanabe, K.; Taniguchi, T.; Tongay, S.; Crommie, M.; Zettl, A.; Wang, F. Optical detection of Mott and generalized Wigner crystal states in WSe_2/WS_2 moiré superlattices. *Nature* **2020**, *579*, 359−363.

(8) Li, H.; Li, S.; Regan, E. C.; Wang, D.; Zhao, W.; Kahn, S.; Yumigeta, K.; Blei, M.; Taniguchi, T.; Watanabe, K.; Tongay, S.; Zettl, A.; Crommie, M.; Wang, F. Imaging two-dimensional generalized Wigner crystals. *Nature* **2021**, *597*, 650−654.

(9) Seyler, K. L.; Rivera, P.; Yu, H.; Wilson, N. P.; Ray, E. L.; Mandrus, D. G.; Yan, J.; Yao, W.; Xu, X. Signatures of moiré-trapped valley excitons in $MoSe_2/WSe_2$ heterobilayers. *Nature* **2019**, *567*, 66−70.

(10) Jia, Y.; Wang, P.; Chiu, C.; Song, Z.; Yu, G.; Jäck, B.; Lei, S.; Klemenz, S.; Cevallos, F. A.; Onyszczak, M.; Fishchenko, N.; Liu, X.; Farahi, G.; Xie, F.; Xu, Y.; Watanabe, K.; Taniguchi, T.; Bernevig, B. A.; Cava, R. J.; Schoop, L. M.; Yazdani, A.; Wu, S. Evidence for a monolayer excitonic insulator. *Nat. Phys.* **2022**, *18*, 87−93.

(11) Onga, M.; Zhang, Y.; Ideue, T.; Iwasa, Y. Exciton Hall effect in monolayer MoS_2. *Nat. Mater.* **2017**, *16*, 1193−1197.

(12) Unuchek, D.; Ciarrocchi, A.; Avsar, A.; Sun, Z.; Watanabe, K.; Taniguchi, T.; Kis, A. Valley-polarized exciton currents in a van der Waals heterostructure. *Nat. Nanotechnol.* **2019**, *14*, 1104−1109.

(13) Li, Z.; Lu, X.; Cordovilla Leon, D. F.; Lyu, Z.; Xie, H.; Hou, J.; Lu, Y.; Guo, X.; Kaczmarek, A.; Taniguchi, T.; Watanabe, K.; Zhao, L.; Yang, L.; Deotare, P. B. Interlayer Exciton Transport in $MoSe_2/WSe_2$ Heterostructures. *ACS Nano* **2021**, *15*, 1539−1547.

(14) Kulig, M.; Zipfel, J.; Nagler, P.; Blanter, S.; Schüller, C.; Korn, T.; Paradiso, N.; Glazov, M. M.; Chernikov, A. Exciton Diffusion and Halo Effects in Monolayer Semiconductors. *Phys. Rev. Lett.* **2018**, *120*, 207401.

(15) Unuchek, D.; Ciarrocchi, A.; Avsar, A.; Watanabe, K.; Taniguchi, T.; Kis, A. Room-temperature electrical control of exciton flux in a van der Waals heterostructure. *Nature* **2018**, *560*, 340−344.

(16) Lee, J.; Mak, K. F.; Shan, J. Electrical control of the valley Hall effect in bilayer MoS_2 transistors. *Nat. Nanotechnol* **2016**, *11*, 421−425.

(17) Shreiner, R.; Hao, K.; Butcher, A.; High, A. A. Electrically controllable chirality in a nanophotonic interface with a two-dimensional semiconductor. *Nat. Photonics* **2022**, *16*, 330−336.

(18) Kim, D.; Seo, M.-K. Experimental Probing of Canonical Electromagnetic Spin Angular Momentum Distribution via Valley-Polarized Photoluminescence. *Phys. Rev. Lett.* **2021**, *127*, 223601.

(19) Branny, A.; Kumar, S.; Proux, R.; Gerardot, B. D. Deterministic strain-induced arrays of quantum emitters in a two-dimensional semiconductor. *Nat. Commun.* **2017**, *8*, 15053.

(20) Luo, Y.; Shepard, G. D.; Ardelean, J. V.; Rhodes, D. A.; Kim, B.; Barmak, K.; Hone, J. C.; Strauf, S. Deterministic coupling of site-

controlled quantum emitters in monolayer WSe_2 to plasmonic nanocavities. *Nat. Nanotechnol.* **2018**, *13*, 1137−1142.
(21) Ye, Y.; Wong, Z. J.; Lu, X.; Ni, X.; Zhu, H.; Chen, X.; Wang, Y.; Zhang, X. Monolayer excitonic laser. *Nat. Photonics* **2015**, *9*, 733−737.
(22) Paik, E. Y.; Zhang, L.; Burg, G. W.; Gogna, R.; Tutuc, E.; Deng, H. Interlayer exciton laser of extended spatial coherence in atomically thin heterostructures. *Nature.* **2019**, *576*, 80−84.
(23) Lien, D. − H.; Amani, M.; Desai, S. B.; Ahn, G. H.; Han, K.; He, J.-H.; Ager, J. W.; Wu, M. C.; Javey, A. Large-area and bright pulsed electroluminescence in monolayer semiconductors. *Nat. Commun.* **2018**, *9*, 1229.
(24) Jauregui, L. A.; Joe, A. Y.; Pistunova, K.; Wild, D. S.; High, A. A.; Zhou, Y.; Scuri, G.; De Greve, K.; Sushko, A.; Yu, C.-H.; Taniguchi, T.; Watanabe, K.; Needleman, D. J.; Lukin, M. D.; Park, H.; Kim, P. Electrical control of interlayer exciton dynamics in atomically thin heterostructures. *Science.* **2019**, *366*, 870−875.
(25) Niehues, I.; Schmidt, R.; Drüppel, M.; Marauhn, P.; Christiansen, D.; Selig, M.; Berghäuser, G.; Wigger, D.; Schneider, R.; Braasch, L.; Koch, R.; Castellanos-Gomez, A.; Kuhn, T.; Knorr, A.; Malic, E.; Rohlfing, M.; Michaelis de Vasconcellos, S.; Bratschitsch, R. Strain Control of Exciton−Phonon Coupling in Atomically Thin Semiconductors. *Nano Lett.* **2018**, *18*, 1751−1757.
(26) Kumar, S.; Kaczmarczyk, A.; Gerardot, B. D. Strain-Induced Spatial and Spectral Isolation of Quantum Emitters in Mono- and Bilayer WSe_2. *Nano Lett.* **2015**, *15*, 7567−7573.
(27) Amani, M.; Lien, D.-H.; Kiriya, D.; Xiao, J.; Azcatl, A.; Noh, J.; Madhvapathy, S. R.; Addou, R.; KC, S.; Dubey, M.; Cho, K.; Wallace, R. M.; Lee, S.-C.; He, J.-H.; Ager, J. W.; Zhang, X.; Yablonovitch, E.; Javey, A. Near-unity photoluminescence quantum yield in MoS_2. *Science* **2015**, *350*, 1065−1068.
(28) Chernikov, A.; van der Zande, A. M.; Hill, H. M.; Rigosi, A. F.; Velauthapillai, A.; Hone, J.; Heinz, T. F. Electrical Tuning of Exciton Binding Energies in Monolayer WS_2. *Phys. Rev. Lett.* **2015**, *115*, 126802.
(29) Tang, H.; Luo, F.; Cui, Z.; Xiao, Y.; Xu, W.; Zhu, Z.; Chen, S.; Wang, X.; Liu, Y.; Wang, J.; Peng, G.; Qin, S.; Zhu, M. Electrically Controlled Wavelength-Tunable Photoluminescence from van der Waals Heterostructures. *ACS Appl. Mater. Interfaces* **2022**, *14*, 19869−19877.
(30) Fang, H. H.; Han, B.; Robert, C.; Semina, M. A.; Lagarde, D.; Courtade, E.; Taniguchi, T.; Watanabe, K.; Amand, T.; Urbaszek, B.; Glazov, M. M.; Marie, X. Control of the Exciton Radiative Lifetime in van der Waals Heterostructures. *Phys. Rev. Lett.* **2019**, *123*, 067401.
(31) Horng, J.; Chou, Y.-H.; Chang, T.-C.; Hsu, C.-Y.; Lu, T.-C.; Deng, H. Engineering radiative coupling of excitons in 2D semiconductors. *Optica.* **2019**, *6*, 1443−1448.
(32) Zhou, Y.; Scuri, G.; Sung, J.; Gelly, R. J.; Wild, D. S.; De Greve, K.; Joe, A. Y.; Taniguchi, T.; Watanabe, K.; Kim, P.; Lukin, M. D.; Park, H. Controlling Excitons in an Atomically Thin Membrane with a Mirror. *Phys. Rev. Lett.* **2020**, *124*, 027401.
(33) Rogers, C.; Gray, D.; Bogdanowicz, N.; Taniguchi, T.; Watanabe, K.; Mabuchi, H. Coherent feedback control of two-dimensional excitons. *Phys. Rev. Research.* **2020**, *2*, 012029.
(34) Sun, Z.; Gu, J.; Ghazaryan, A.; Shotan, Z.; Considine, C. R.; Dollar, M.; Chakraborty, B.; Liu, X.; Ghaemi, P.; Kéna-Cohen, S.; Menon, V. M. Optical control of room-temperature valley polaritons. *Nat. Photonics* **2017**, *11*, 491−496.
(35) Dufferwiel, S.; Lyons, T. P.; Solnyshkov, D. D.; Trichet, A. A. P.; Withers, F.; Schwarz, S.; Malpuech, G.; Smith, J. M.; Novoselov, K. S.; Skolnick, M. S.; Krizhanovskii, D. N.; Tartakovskii, A. I. Valley-addressable polaritons in atomically thin semiconductors. *Nat. Photonics* **2017**, *11*, 497−501.
(36) Chen, Y.-J.; Cain, J.; Stanev, T. K.; Dravid, V. P.; Stern, N. P. Valley-polarized exciton−polaritons in a monolayer semiconductor. *Nat. Photonics* **2017**, *11*, 431−435.
(37) Akselrod, G. M.; Argyropoulos, C.; Hoang, T. B.; Ciracì, C.; Fang, C.; Huang, J.; Smith, D. R.; Mikkelsen, M. H. Probing the mechanisms of large Purcell enhancement in plasmonic nanoantennas. *Nat. Photonics* **2014**, *8*, 835−840.
(38) Akselrod, G. M.; Ming, T.; Argyropoulos, C.; Hoang, T. B.; Lin, Y.; Ling, X.; Smith, D. R.; Kong, J.; Mikkelsen, M. H. Leveraging Nanocavity Harmonics for Control of Optical Processes in 2D Semiconductors. *Nano Lett.* **2015**, *15* (5), 3578−3584.
(39) Han, C.; Ye, J. Polarized resonant emission of monolayer WS_2 coupled with plasmonic sawtooth nanoslit array. *Nat. Commun.* **2020**, *11*, 703.
(40) Li, Z.; Liu, C.; Rong, X.; Luo, Y.; Cheng, H.; Zheng, L.; Lin, F.; Shen, B.; Gong, Y.; Zhang, S.; Fang, Z. Tailoring MoS_2 Valley-Polarized Photoluminescence with Super Chiral Near-Field. *Adv. Mater.* **2018**, *30*, 1801908.
(41) Wu, Z.; Li, J.; Zhang, X.; Redwing, J. M.; Zheng, Y. Room-Temperature Active Modulation of Valley Dynamics in a Monolayer Semiconductor through Chiral Purcell Effects. *Adv. Mater.* **2019**, *31*, 1904132.
(42) Ren, H.; Briere, G.; Fang, X.; Ni, P.; Sawant, R.; Héron, S.; Chenot, S.; Vézian, S.; Damilano, B.; Brändli, V.; et al. Metasurface orbital angular momentum holography. *Nat. Commun.* **2019**, *10*, 2986.
(43) Meinzer, N.; Barnes, W.; Hooper, I. Plasmonic meta-atoms and metasurfaces. *Nat. Photonics* **2014**, *8*, 889−898.
(44) Jun, Y.; Huang, K.; Brongersma, M. Plasmonic beaming and active control over fluorescent emission. *Nat. Commun.* **2011**, *2*, 283.
(45) Zheng, G.; Mühlenbernd, H.; Kenney, M.; Li, G.; Zentgraf, T.; Zhang, S. Metasurface holograms reaching 80% efficiency. *Nat. Nanotechnol.* **2015**, *10*, 308−312.
(46) Kim, B.; Luo, Y.; Rhodes, D.; Bai, Y.; Wang, J.; Liu, S.; Jordan, A.; Huang, B.; Li, Z.; Taniguchi, T.; Watanabe, K.; Owen, J.; Strauf, S.; Barmak, K.; Zhu, X.; Hone, J. Free Trions with Near-Unity Quantum Yield in Monolayer $MoSe_2$. *ACS Nano* **2022**, *16*, 140−147.
(47) Selig, M.; Berghäuser, G.; Raja, A.; Nagler, P.; Schüller, C.; Heinz, T. F.; Korn, T.; Chernikov, A.; Malic, E.; Knorr, A. Excitonic linewidth and coherence lifetime in monolayer transition metal dichalcogenides. *Nat. Commun.* **2016**, *7*, 13279.
(48) Huang, Z.; Liu, Y.; Dini, K.; Tan, Q.; Liu, Z.; Fang, H.; Liu, J.; Liew, T.; Gao, W. Robust Room Temperature Valley Hall Effect of Interlayer Excitons. *Nano Lett.* **2020**, *20*, 1345−1351.
(49) Kim, H.; Uddin, S. Z.; Higashitarumizu, N.; Rabani, E.; Javey, A. Inhibited nonradiative decay at all exciton densities in monolayer semiconductors. *Science* **2021**, *373*, 448−452.
(50) Lien, D.-H.; Uddin, S. Z.; Yeh, M.; Amani, M.; Kim, H.; Ager, J. W.; Yablonovitch, E.; Javey, A. Electrical suppression of all nonradiative recombination pathways in monolayer semiconductors. *Science* **2019**, *364*, 468−471.

https://doi.org/10.1021/acs.nanolett.2c04604
Nano Lett. XXXX, XXX, XXX−XXX